The Astrophysical Journal, 613:151–158, 2004 September 20

SYNCHROTRON VERSUS COMPTON INTERPRETATIONS FOR EXTENDED X-RAY JETS

Armen Atoyan
Centre de Recherches Mathématiques, Université de Montréal, Montreal, QC H3C 3J7, Canada; atoyan@crm.umontreal.ca

and

Charles D. Dermer
E. O. Hulburt Center for Space Research, Code 7653, Naval Research Laboratory, Washington, DC 20375-5352; dermer@gamma.nrl.navy.mil
Received 2004 February 25; accepted 2004 May 10

ABSTRACT

A widely discussed explanation for the origin of the X-ray emission observed from knots in extended quasar jets with the *Chandra X-Ray Observatory* is Compton-scattered cosmic microwave background radiation by electrons with Lorentz factors $\gamma' \sim 10^2$. This model faces difficulties in terms of total energy requirements and in explaining the spatial profiles of the radio, optical, and X-ray knots in sources such as PKS 0637−752, 3C 273, or PKS 1127−145. These difficulties can be resolved in the framework of one- and two-component synchrotron models. We propose a model in which the broadband radio–to–X-ray synchrotron emission in quasar jets is powered by collimated beams of ultrahigh energy neutrons and γ-rays formed in the subparsec-scale jets. The decay of the neutral beam in the intergalactic medium drives relativistic shocks to accelerate nonthermal electrons of the ambient medium. A second synchrotron component arises from the injection of leptons with Lorentz factors $\gg 10^7$ that appear in the extended jet in the process of decay of ultrahigh energy γ-rays. This approach could account for qualitative differences in the extended X-ray jets of Fanaroff-Riley (FR) 1 and 2 galaxies. Detection of high-energy neutrinos from blazars and core-dominated quasars will provide strong evidence for this model.

Subject headings: galaxies: active — galaxies: jets — gamma rays: theory — radiation mechanisms: nonthermal — X-rays: galaxies

1. INTRODUCTION

Three main radiation processes considered to account for the nonthermal X-ray emission in knots and hot spots of the extended jets discovered by the *Chandra X-Ray Observatory* are synchrotron, synchrotron self-Compton (SSC), and Compton scattering of external photons contributed mostly by the CMBR (cosmic microwave background radiation; e.g., Harris & Krawczynski 2002; Stawarz 2004). In X-ray knots of quasar jets with deprojected lengths $\gtrsim 100$ kpc, where the X-ray spectrum is not a smooth extension of the radio-optical spectrum, a currently favored interpretation is the external Compton (EC) model (Tavecchio et al. 2000; Celotti et al. 2001). In this model, the X-ray emission from knots such as WK 7.8 of PKS 0637−752 is argued to be due to cosmic microwave background photons that are Compton-upscattered by nonthermal electrons from kiloparsec-scale emitting regions in bulk relativistic motion at distances up to several hundred kpc away from the central engine.

We note, however, that in the framework of this model it is problematic to explain a clear trend observed in many extended jets of radio quasars, such as those of 3C 273 (Marshall et al. 2001; Sambruna et al. 2001) or those of PKS 1127−145 (Siemiginowska et al. 2002), namely, that the X-ray brightness of the knots decreases with distance along the jet while the radio flux is *increasing*. The Lorentz factors of the X-ray–emitting electrons in the EC model are smaller than those of the radio- and optical-emitting electrons. It is therefore difficult to explain comparable knot sizes at optical and X-ray frequencies but extended emission at radio frequencies. Moreover, the radiative cooling of these low-energy electrons is slow, resulting in high total energy requirements.

In this paper we examine these difficulties and propose an alternative interpretation for X-ray emission from knots in Fanaroff-Riley (FR) 2 radio galaxy jets and quasars for which the radio through X-ray fluxes are explained by synchrotron radiation from one or two components of relativistic electrons. Both of these components are powered by neutral beams of ultrahigh energy (UHE) neutrons and γ-rays produced by the jet at the base of the central active galactic nucleus (AGN) engine (Atoyan & Dermer 2001, 2003). The momentum of the decaying beam of neutrons drives a relativistic shock that accelerates electrons from the surrounding medium to produce the main nonthermal electron component responsible for the broadband radio–optical–X-ray synchrotron emission. In such sources, a second ultrarelativistic lepton component can also be injected from neutron β-decay and the pair production by UHE γ-rays attenuated by the CMBR. The synchrotron emission of these pairs can contribute to or even dominate the synchrotron X-ray flux in the knots of core-dominated quasars.

Here we focus on knots in quasar jets, although the same two-component synchrotron model can apply to terminal hot spots of FR 2 galaxies such as Cyg A (Wilson et al. 2000) or Pic A (Wilson et al. 2001), in which the SSC process could also play a role. For the X-ray jets in FR 1 sources, with deprojected lengths of only $\lesssim 5$ kpc, X-ray and optical emission are generally consistent with a smooth power-law continuation of the radio spectrum, indicating a synchrotron radiation origin. Mild spectral hardenings at X-ray energies, such as those observed in the knots of M87's jet (Wilson & Yang 2002; Marshall et al. 2002), could still be explained within the context of a single-component synchrotron model (Dermer & Atoyan 2002, hereafter DA02). In FR 1 galaxies and BL Lac objects, the neutral beam power is considerably smaller than in FR 2 galaxies

and quasars because of the weaker external radiation field in the inner jet (Atoyan & Dermer 2001), so that extended jets in FR 1 galaxies would primarily result from the jet plasma expelled directly from the central nucleus.

In § 2 we discuss the difficulties with the EC model, and we propose one- and two-component synchrotron models for the X-ray jets in § 3. The rationale for the model is discussed in § 4, including testable predictions from X-ray and high-energy neutrino observations and a brief discussion of this model in the context of a scenario for AGN evolution.

2. DIFFICULTIES WITH THE EC MODEL

The principal reason for difficulties of the EC model is that the Lorentz factors $\gamma = E/m_e c^2$ of electrons that produce X-rays by Compton scattering on CMBR are rather small. Electrons that produce synchrotron radio emission at observer-frame frequencies ν have comoving-frame Lorentz factors $\gamma'_{\rm syn} \approx 10^3[(\nu/{\rm GHz})(1+z)/\delta_{10}B_{30}]^{1/2}$, where $\delta = [\Gamma(1-\beta\cos\theta)]^{-1} \equiv 10\delta_{10}$ is the Doppler factor of the emitting knot moving with Lorentz factor $\Gamma = (1-\beta^2)^{-1/2}$ at an angle θ to the observer and $B_{30} \equiv B'/(30\ \mu{\rm G}) \gtrsim 1$ is a characteristic magnetic field in the knot derived from equipartition arguments.[1] Electrons that Compton-scatter the CMBR to observed X-ray energies $E_{\rm keV} = E_{\rm X}/1$ keV have $\gamma'_{\rm C} \approx 90(E_{\rm keV})^{1/2}/\delta_{10}$. Consequently, the X-ray–emitting electrons cool more slowly than the radio-emitting electrons. Converting the comoving Compton cooling time $t'_{\rm C} = t_{\rm C}/\Gamma \simeq 1.8\times10^{12}[(1+z)^4\gamma'\Gamma^2]^{-1}$ yr into the stationary frame, we find that for the X-ray–emitting electrons,

$$t_{\rm C} \cong 2.2\times10^9\,\frac{\delta}{\Gamma}E_{\rm keV}^{-1/2}(1+z)^{-4}\ {\rm yr}\ . \qquad (1)$$

The coefficient in this timescale corresponds to a propagation distance of ≈630 Mpc, which is orders of magnitude larger than the jet extent. This implies a very inefficient extraction of the injected electron energy. Note also that the efficiency for Compton production of the observed X-ray flux cannot be essentially improved by assuming $\Gamma \gg 1$, as suggested earlier (Tavecchio et al. 2000), since $\delta \sim \Gamma$ for the energetically most favorable ("not debeamed") orientation of the jet, as shown in the next section.

This leads to large total energy requirements, as well as to a number of difficulties in the interpretation of spectra and spatial profiles and sizes of the resolved knots in the radio and X-ray domains.

2.1. *Total Energy Requirements*

The total electron energy required to produce the νF_ν X-ray flux $f_{\rm X} = 10^{-13} f_{-13}$ ergs cm^{-2} s^{-1} can be calculated by noting that the comoving luminosity of a single electron with Lorentz factor $\gamma'_{\rm C}$ is $(-dE'/dt')_{\rm C} = 4c\sigma_{\rm T}u'_0\gamma'^2_{\rm C}/3$, where $u'_0 = (4\Gamma^2/3)\hat{u}_{\rm CMB}(1+z)^4$ is the comoving energy density of the CMBR when $\Gamma \gg 1$ and $\hat{u}_{\rm CMB} = 4\times10^{-13}$ ergs cm^{-3} is the local CMBR energy density. The comoving power $L'_{\rm X} = N_e(-dE'/dt')_{\rm C} \cong 32\pi d^2\Gamma^2 f_{\rm X}/\delta^6$ (see eq. [39] in Dermer & Schlickeiser 2002), where $N_e = N'_e$ is the total number of relativistic electrons with $\gamma' \sim \gamma'_{\rm C}$ and $d = 10^{28}d_{28}$ cm is the luminosity distance. This gives for the total energy in the stationary frame

$$W_e \simeq N_e\gamma'_{\rm C}m_e c^2\Gamma \simeq 2.2\times10^{61}\,\frac{f_{-13}d_{28}^2\Gamma}{\sqrt{E_{\rm keV}}(1+z)^4\delta^5}\ {\rm ergs}. \qquad (2)$$

[1] Primes refer to comoving quantities, although B is always referred to in the proper frame.

Note that this derivation takes into account the directionality of target photons when an isotropic radiation field in the stationary frame is transformed to the comoving frame (Dermer 1995; Dermer et al. 1997). Neglecting this effect gives results accurate within a factor of ∼2 when $\delta \approx \Gamma$ but can introduce large errors when $\delta \ll \Gamma$.

The energy given in equation (2) accounts only for electrons with $\gamma' \sim \gamma'_{\rm C}$ and neglects the protons normally required to ensure neutrality. Since the proton energy even at rest is ≳10 times larger than the comoving energy of electrons with $\gamma'_{\rm C} \sim 100$, the total energy of particles $W_{\rm tot} \gtrsim 10W_e$ is needed, unless e^+-e^-–pair-dominated plasma could be formed in the knot. Celotti & Fabian (1993) argue, however, that quasar jets are composed of electron-proton plasma by comparing jet luminosities inferred from SSC models with the radio lobe powers.

The total energy requirements can be reduced to reasonable values for X-ray knots with a typical size of $R_{\rm kpc} = R/$ kpc ~ 1 only by assuming $\delta \sim \Gamma \gtrsim 10$. For a jet moving at an angle θ with respect to the line of sight, the maximum Doppler factor is $\delta_{\rm max} = 1/\sin\theta$, which is reached if in addition $\Gamma = 1/\sin\theta$. This implies very small inclination angles of jets up to $\theta \leq 1/\Gamma \lesssim 5^\circ$ to have $\delta \gtrsim 10$.

For knot WK 7.8 in PKS 0637−752 at $z = 0.651$, $d_{28} = 1.20$ (for a ΛCDM cosmology with $\Omega_m = 0.3$, $\Omega_\Lambda = 0.7$, and Hubble constant of 70 km s^{-1} Mpc^{-1}), and $f_{-13} \approx 0.4$ (from Schwartz et al. [2000], including bolometric correction for the integral flux), equation (2) results in $W_e \simeq 2\times10^{56}$ ergs and $W_{\rm tot} \gg 10^{57}$ ergs in the stationary frame, if one assumes $\theta \simeq 5^\circ$ and $\Gamma \approx \delta \cong 10$.

For 3C 273 at $z = 0.158$ and $d_{28} = 0.23$, the angle $\theta \cong 17^\circ$ explains the superluminal motion of the subparsec jet (Roland et al. 1994), and it may be as large as $\simeq 30^\circ$–35° for the kiloparsec-scale jet, as deduced from polarization measurements by Conway & Davis (1994). Even taking $\theta = 17^\circ$ for knot A1 with measured bolometric flux $f_{-13} \simeq 3$ in the keV region (Marshall et al. 2001), the minimum electron energy when $\Gamma = \delta = 3.4$ is $W_e \gtrsim 1.4\times10^{58}$ ergs for the *Chandra* observations. This implies a total energy $W_{\rm tot} \gtrsim 10^{59}$ ergs in the stationary frame, or $W'_{\rm tot} \simeq W_{\rm tot}/\Gamma > 10^{58}$ ergs in the comoving frame.

For an X-ray knot of size $R_{\rm kpc} \sim 1$, an equipartition magnetic field for the comoving energy $W'_{\rm tot} = 10^{56}W'_{56}$ ergs is $B'_{\rm eq} \cong 150(W'_{56})^{1/2}R_{\rm kpc}^{-3/2}\ \mu$G. For knot WK 7.8 in PKS 0637−752, the size $R_{\rm kpc} \approx 1$ kpc, corresponding to FHWM $\Delta\theta = 0\farcs3$ [but not $R \simeq 3$ kpc, as in Tavecchio et al. (2000), if one takes into account the redshift effect, $R = d\theta/(1+z)^2$] and $W'_{56} \approx 0.2$ in the case of $\delta = \Gamma = 10$. This results in the equipartition magnetic field $B'_{\rm eq} \approx 70\ \mu$G (instead of $\simeq 15\ \mu$G for the 3 times larger knot size). This field is unacceptably high for the EC model because it would overproduce the observed radio flux, given the number of electrons with $\gamma' \sim \gamma'_{\rm C}$ needed for the X-ray flux. However, in the case of magnetic fields at the level of only a few tens of μG, the energy density, and thus the pressure of relativistic particles, would be much higher than the pressure of the magnetic field. Therefore, either the confinement time of electrons in the knot would be $t'_{\rm conf} \sim R/(c/\sqrt{3}) \simeq 2\times10^{11}R_{\rm kpc}$ s or else the knot would be inflating on the same timescale. This implies a comoving injection power in the knot of $L' \gtrsim 5\times10^{44}W'_{56}/R_{\rm kpc}$ ergs s^{-1} or a stationary-frame injection power $\Gamma^2L' \gtrsim 10^{47}$ ergs s^{-1}. In fact, taking into account the contribution of protons, Tavecchio et al. (2000) require a power of 3×10^{48} ergs s^{-1} to model the spectral energy distribution (SED) of knot WK 7.8 of PKS 0637−752 with the EC model. Although they argue that this is consistent

with the total kinetic power of the jets inferred to power the giant radio lobes of radio galaxies, the largest jet power in the sample of Rawlings & Saunders (1991) hardly exceeds 10^{47} ergs s^{-1}. This power also is 1–2 orders of magnitude greater than the maximum peak γ-ray luminosities inferred from EGRET observations of blazars, taking into account the likely beaming factor of $\sim$1% (Mukherjee & Chiang 1999).

It should be noted here that in principle it is possible to satisfy the equipartition condition also for a given size $R =$ 1 kpc of the knot WK 7.8, increasing the Doppler factor δ further to $\simeq$20 (Dermer & Atoyan 2004). This will also minimize the power requirements for the EC model (Ghisellini & Celotti 2001; Dermer & Atoyan 2004). However, this is possible only if the jet inclination angle is further decreased, to $\leq 3^\circ$. Although this cannot be excluded for a particular source, such angles would be problematic to assume for many sources, as we discuss in § 4.

2.2. *X-Rays versus Radio Spatial and Spectral Profiles*

In the EC CMBR model, X-rays are produced by electrons with $\gamma_C \sim 10^3$ in the stationary frame. They cool on the CMBR only on gigayear timescales $t_{cool} \simeq t_C$ of equation (1), unless their overall cooling is dominated by synchrotron losses, which would then overproduce the observed radio flux at low frequencies. Since the photon target for the Compton process does not degrade at any distance r from the parent AGN, the strong fading of the X-ray knots and the jet itself (i.e., outside the knots) with r in many FR 2 quasars, such as in 3C 273 (Sambruna et al. 2001; Marshall et al. 2001), PKS 1127−145 (Siemiginowska et al. 2002), or Pic A (Wilson et al. 2001), implies either a fast decrease of the total number of electrons with $\gamma \sim \gamma_C$ or a decline of the jet Doppler factor. Because the observed radio emission is produced by electrons with γ_{syn} larger than γ_C by only a factor $\lesssim$10, both assumptions would imply a rapid fading of the radio brightness with distance as well. Meanwhile, exactly the opposite radio brightness profiles are observed.

Furthermore, because the cooling time is shorter for radio than for Compton X-ray–emitting electrons, one should also expect that the X-ray knots in the EC model would be more diffuse than the radio or optical knots. Again, this prediction is in disagreement with observations. Note in this regard that the adiabatic cooling of X-ray–emitting electrons due to fast expansion of X-ray knots, as proposed recently (Tavecchio et al. 2003) for the interpretation of the fading of the X-ray brightness outside the knots, would also equally impact the radio-emitting electrons (Stawarz et al. 2004). Therefore, this scenario would not resolve either of these two discrepancies between the X-ray and the radio brightness patterns.

One more difficulty for the Compton interpretation arises for those jets whose spectral indices α (for the spectral flux $F_\nu \propto \nu^{-\alpha}$) are significantly different at radio and X-ray frequencies. As also discussed earlier, e.g., by Harris & Krawczynski (2002), spectral profiles steeper in X-rays than in radio, with $\alpha_X > \alpha_r$, and especially jets or knots in a number of FR 1 galaxies with $\alpha_X \gtrsim 1$, represent strong evidence for the synchrotron origin of the X-ray flux, implying acceleration of electrons with $\gamma' \gg 10^7 [E_{keV}(1+z)/\delta_{10}B_{30}]^{1/2}$ in the knots of radio jets. This also is the case for many terminal hot spots, such as the western hot spot of Pic A, with $\alpha_r \approx 0.74$ and $\alpha_X = 1.07 \pm 0.11$ (Wilson et al. 2001).

It should be pointed out here that these difficulties with the interpretation of different spectral and opposite spatial profiles in radio and X-ray patterns of jets relate not only to EC models but equally to SSC models. The X-ray flux in SSC models is likewise produced by low-energy electrons that emit the synchrotron radio photons for subsequent Compton interactions, and the density of this target does not decline but may even increase along the jet.

3. SYNCHROTRON ORIGIN OF X-RAYS

In the X-ray jets of FR 1 galaxies, such as 3C 66B (Hardcastle et al. 2001) and some knots in M87's jet (Wilson & Yang 2002; Marshall et al. 2002), the X-ray–optical–radio spectra are consistent with a single or smoothly steepening power-law spectrum, which is readily explained by a single-component synchrotron spectrum. It is a common pattern that the peaks of the emission of the knots and hot spots in the radio, optical, and X-ray domains of quasar jets are well correlated and often coincide, as in the jet of 3C 273 (Sambruna et al. 2001; Marshall et al. 2001). When the profiles do not coincide, as in the FR 1 galaxy M87 (Wilson & Yang 2002) or the GPS quasar PKS 1127−145 (Siemiginowska et al. 2002), the peak emission of the X-ray profile is closer to the core than the radio profile.

This behavior suggests a common synchrotron origin for the radiation in all bands, in which nonthermal electrons accelerated at a shock lose energy through adiabatic and radiative processes as they flow downstream from the shock. The synchrotron optical and X-ray emissions from the highest energy electrons have roughly coincident profiles, but the radio emission is far more extended because of the longer cooling timescale and can even be offset as a consequence of a low-energy cutoff in the electron injection function.[2]

In apparent conflict with a synchrotron model are the SEDs of many quasar knots and hot spots that show a general behavior whereby the optical spectra are steeper than both the radio and the X-ray spectra and whereby the X-ray fluxes are above the extrapolation from the optical band. This behavior cannot be immediately explained by a "standard" synchrotron model with a single power-law electron component. It apparently requires a second electron component at very high energies $\gtrsim$10 TeV with a sharp cutoff at lower energies. However, the origin of such electrons in the knot is not easy to understand and obviously needs an explanation.

3.1. *Single-Component Model*

In our model (DA02), we have shown that in many cases even a single population of electrons with a power-law injection spectrum $Q_{inj}(\gamma') \propto \gamma'^{-p} e^{-\gamma'/\gamma'_{max}}$ could explain the observed spectral peculiarities if the electrons are accelerated to sufficiently high energies with $\gamma'_{max} = E'_{max}/m_e c^2 \gtrsim 10^8$. When CMBR cooling in the Thomson regime exceeds synchrotron cooling, i.e., when the magnetic and radiation field energy densities relate as $u'_0 = \hat{u}_{CMB}(1+z)^4(4\Gamma^2/3) \gtrsim u'_B = (B')^2/8\pi$, a hardening in the electron spectrum is formed at comoving electron energies $\gamma' \gtrsim 10^8/\Gamma(1+z)$, where Klein-Nishina (KN) effects in Compton losses become important. The spectrum steepens again at higher energies when synchrotron losses take over. For B' up to a few tens of μG, this condition is satisfied for jets with $\Gamma \gtrsim 10$. Such an effect produces a hardening in the synchrotron spectrum between optical and X-ray frequencies.

In Figure 1 we show fits to the multiwavelength SEDs of knots A1 and B1 of the jet of 3C 273, with deprojected length

[2] Georganopoulos & Kazanas (2004) explain this offset in the context of an EC model in which the flow decelerates downstream from the injection site, but they must require that the magnetic field be amplified through compression in the downstream decelerating flow.

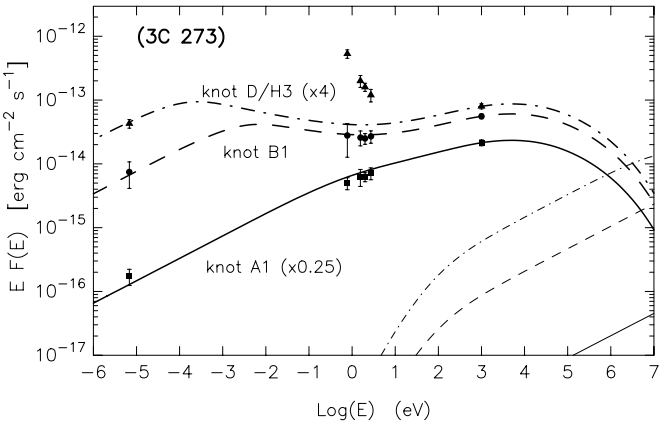

FIG. 1.—SED fits to the broadband fluxes of knots A1, B1, and D/H3 in the jet of 3C 273, calculated in the framework of single-component synchrotron model of DA02. For knots D/H3 and A1, the measured fluxes (Marshall et al. 2001) are displaced up and down by a factor of 4, respectively, to avoid overlaps in the optical band. The electron injection rates provide the observed X-ray fluxes at 1 keV. For all knots most of the model parameters are assumed the same (see text): electron injection spectrum with $p = 2.3$ and high and low cutoff energies $\gamma'_{\rm max} = 2 \times 10^8$ and $\gamma'_{\rm min} = 2 \times \Gamma$, respectively, $B = 15$ μG, $\Gamma_{\rm knot} = 15$, and $\theta_{\rm jet} = 17^\circ$ (resulting in $\delta_{\rm knot} \simeq 1.5$). The main difference is in the different escape (or else effective injection) times for the various knots, namely, $t'_{\rm esc,\,A1} = 1.6 \times 10^3$, $t'_{\rm esc,\,B1} = 3.8 \times 10^4$, and $t'_{\rm esc,\,D/H3} = 1.5 \times 10^5$ yr. The solid, dashed, and dash-dotted curves show the fluxes of EC radiation on CMBR for these parameters of knots.

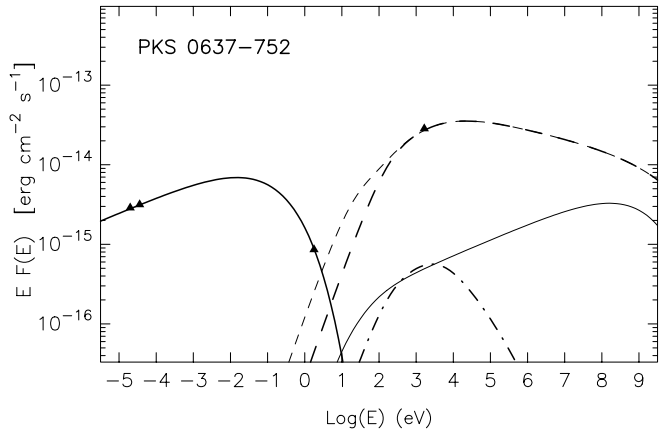

FIG. 2.—Spectral fits to the fluxes of knot WK 7.8 of PKS 0637−752 (Schwartz et al. 2000; Chartas et al. 2000), calculated in the framework of a two-component synchrotron model, assuming $B' = 100$ μG, $\Gamma = 5$, and $\theta_{\rm jet} = 10^\circ$ for the jet. The heavy solid curve shows the synchrotron flux from the first electron component with the injection index $p_1 = 2.6$, the exponential cutoff above $\gamma'_{1,\,\rm max} = 1.8 \times 10^5$, and a cutoff below $\gamma'_{1,\,\rm min} \simeq 20$. The thin solid curve shows Compton fluxes from these electrons. For the second electron component, an injection spectrum with $p_2 = 2.2$ at energies $2 \times 10^7 \lesssim \gamma' \lesssim 10^{11}$ and cutoffs outside this interval are assumed. The heavy dashed curve shows the synchrotron radiation of this component, and the dot-dashed curve shows the radiation from the pair-photon cascade initiated by the second electron component in the knot. An electron escape time of $t'_{\rm esc} = 1$ kyr is assumed. For comparison, the thin dashed curve shows the flux of the second component in the case $t'_{\rm esc} = 3$ kyr.

more than 100 kpc, calculated in the framework of a single-component synchrotron model (DA02). For all knots, $B = 15$ μG (including the knot D/H3), and practically all other model parameters are also the same. The single parameter that is different for the three curves is the time from the start of electron injection, which can also be interpreted as the different escape times of electrons from the knots. These times are given in the figure caption. The curves are normalized to the observed X-ray fluxes at 1 keV. The total electron energies in knots A1 and B1 are $W'_{e,\,\rm A1} = 1.3 \times 10^{56}$ and $W'_{e,\,\rm B1} = 1.6 \times 10^{57}$ ergs, respectively, and the required electron injection powers are $L'_{e,\,\rm A1} = 2 \times 10^{45}$ and $L'_{e,\,\rm B1} = 1.3 \times 10^{45}$ ergs s^{-1}, respectively.

Note that the spectra in Figure 1 are fitted for the jet inclination angle $\theta = 17^\circ$ in 3C 273. For the assumed Lorentz factor $\Gamma = 15$, this angle is much larger than the effective beaming angle of the inner jet emission $\theta_{\rm beam} \cong 57^\circ/\Gamma$ and results in $\delta \approx 1.5 \ll \Gamma$. Even for this strongly debeamed case, the simple "one-zone and single-component" synchrotron model provides good fits to the observed fluxes of the knots A1 and B1 with still acceptable total energy requirements. The curves in Figure 1 show the fluxes to be expected from the EC process for the same model parameters. It follows from comparing these fluxes with the observed X-ray fluxes that for the given parameters of 3C 273, the EC model would require 2–3 orders of magnitude more total energy for both knots A1 and B1. Even if we formally assume an unreasonably large injection/escape time, however, it is not possible to explain the SED of knot D/H3 in the framework of a single-component synchrotron model.

3.2. *Second Electron Component*

The X-ray emission in knot D/H3 of 3C 273, or generally in knots in which either the optical flux is very steep, $\alpha_{\rm opt} \gtrsim 1.5$, or the energy flux νF_ν is much higher in X-rays than in the optical band, can be explained only by synchrotron radiation, either as a second component of electrons or, as another possibility, as synchrotron emission of UHE protons with $\gamma_p \gtrsim 10^9$ and magnetic fields as strong as $B_{\rm mG} = B/10^{-3}$ G $\gtrsim 1$ (Aharonian 2002).

The energy requirements of the proton synchrotron model are as demanding as those of the Compton model. In this model, keV radiation is produced by protons with comoving Lorentz factors $\gamma'_p \simeq 4 \times 10^8$ $[E_{\rm keV}(1+z)/B'_{\rm mG}\delta]^{1/2}$. The synchrotron cooling time of these protons $t'_{\rm sp} \simeq 1.5 \times 10^{17}/(B^2_{\rm mG}\gamma'_p)$ yr which, in the stationary frame, is

$$t_{\rm sp} = 3.8 \times 10^8 \Gamma \delta^{1/2} E_{\rm keV}^{-1/2} B_{\rm mG}^{-3/2} (1+z)^{-1/2} \ {\rm yr}. \qquad (3)$$

Comparing this time with that of equation (1) shows that the energy required in UHE protons alone in the knot should be practically as large as in electrons with $\gamma' \sim \gamma'_{\rm C}$ in the EC model. At the same time, one also has to assume that only a small amount of energy is injected in radio electrons not to overproduce the observed radio flux in the high magnetic field in the knot.

The origin of the second electron component to produce X-ray synchrotron radiation in a leptonic model may, however, seem ad hoc. Noticeably, this second electron component should be concentrated mostly at multi-TeV and higher energies, with a cutoff at energies below $\gamma' \sim 10^7$, or otherwise the synchrotron flux of this component would exceed the observed flux in the optical band. After discussing in this section the requirements and demonstrating the feasibility of a two-component synchrotron model, we propose a scenario for the origin of the second component in § 3.3.

In Figure 2 we show a fit to the SED of knot WK 7.8 of PKS 0637−752, calculated in the framework of a two-component synchrotron model. We assume a power-law spectrum with $p_1 = 2.6$ to fit the radio spectrum and an exponential cutoff above $\gamma'_{1,\,\rm max} = 1.8 \times 10^5$, which explains the steep optical flux. The injection spectrum of the second electron component has a

power-law index of $p_2 = 2.2$, with exponential cutoffs below $\gamma'_{2,\min} = 2\times10^7$ and above $\gamma'_{2,\max} = 10^{11}$. The synchrotron radiation of this second electron component is shown by the heavy dashed curve for the escape time $t'_{\rm esc} = 1$ kyr. For comparison, the thin dashed curve shows the evolution of the fluxes in the case of a larger escape time of the electrons from the knot, with $t'_{\rm esc} = 3$ kyr. As can be seen, further increase of this parameter beyond $t'_{\rm esc} \simeq 10^4$ yr when $B' = 100$ μG would result in the synchrotron flux of the rapidly cooling second electron component exceeding the observed flux in the optical band.

Longer escape/injection times $t'_{\rm esc} \gtrsim 3$ kyr are allowed for smaller magnetic fields, $\lesssim 100$ μG, in knot WK 7.8. The interpretation of these timescales when $t'_{\rm esc} \sim 3$–10 kyr suggests that X-ray knots are manifestations of relativistic shock waves with transverse size scales of kiloparsec dimensions that are moving toward us (although generally at some angle $\theta \sim 10^\circ$–20°) with $\Gamma \sim 10$. These shocks accelerate electrons and can amplify the magnetic field in the downstream flow. In the shocked material, the relativistic plasma expands at speeds close to $c/\sqrt{3}$ (in the shock frame). Then the escape times $t'_{\rm esc} \sim 3$–10 kyr would imply an effective thickness of the region with enhanced magnetic fields downstream of the shock equal to about $h \simeq (c/\sqrt{3})t'_{\rm esc} \sim 1$ kpc. This is comparable to the given transverse size of the shock, and therefore, even smaller escape times could still be reasonable.

It is important that the energy requirements derived for the first and second electron components are low. For the assumed parameters of knot WK 7.8, the total comoving energy in the first component is $W'_{e,1} = 3.9\times10^{55}$ ergs and only $W'_{e,2} = 5.5\times10^{51}$ ergs in the second component. The energetics $W'_{e,1}$ of the first component is contributed mostly by radio-emitting electrons that cool slowly and can be accumulated in a larger region over a longer time than the value $t'_{\rm esc} \simeq 1$ kyr assumed in Figure 2. Comparing the EC flux shown by the thin solid line with the observed X-ray flux, one can see that the chosen parameters for knot WK 7.8 would require in the EC model a total energy budget larger by 2 orders of magnitude than that found in Figure 2, namely, $W_e \simeq \Gamma W'_e > 10^{58}$ ergs. It would also require a magnetic field well below the nearly equipartition value assumed in Figure 2 to reduce the radio emissivity.

For the fast-cooling second component of electrons, a more informative measure than $W_{e,2}$ is the comoving injection power, or injection "luminosity" $L'_{e,2} = 10^{43}L'_{43}$ ergs s^{-1}. The model fitted to the observed X-ray flux in Figure 2 requires $L'_{43} = 0.3$. This luminosity implies that electrons with average Lorentz factor $\gamma'_8 = \gamma'/10^8 \simeq 1$ are injected at the rate

$$\dot{N}'_{e,2} \simeq 10^{41}L'_{43}(\gamma'_8)^{-1}\ {\rm s}^{-1}. \quad (4)$$

Because of the relativistic time contraction $dt' = dt/\Gamma$, this injection rate becomes even smaller in the stationary frame, $\dot{N}_{e,2} = \dot{N}'_{e,2}/\Gamma$.

The steep spectra of the first electron component with the power-law injection index $p = 2.6$–2.7 needed to explain the radio fluxes of the knot WK 7.8 imply that the shock is not very strong. This is in good agreement with the relatively low value of the characteristic maximum energy for the first electron component, $\gamma'_{1,\max} = 1.8\times10^5$ in Figure 2. But then the production of a second electron component reaching much higher energies appears to be problematic.

3.3. *Model for the Second Electron Component*

The problem is solved if the second electron component is not accelerated by the shock but rather is swept up in the upstream plasma. Spectra of electrons of the type required, with a sharp cutoff below multi-TeV energies, could appear in knots at distances from a few tens to $\gg 100$ kpc from the decaying neutral beam of UHE neutrons and γ-rays produced in the relativistic compact jet of AGNs at subparsec scales, as we have recently suggested (Atoyan & Dermer 2001, 2003). The total power transported by such a beam in FR 2 quasars to distances of 0.1–1 Mpc can be very significant. The energy released in UHE neutrons at energies of $\sim10^{17}$–10^{20} eV can range from a few to several percent of the entire energy of protons accelerated by the inner jet (Atoyan & Dermer 2003).

The total number of electrons in the second component is so small that even the number of β-decay electrons from the decay of neutrons could be sufficient for equation (4). The decay lifetime of neutrons at rest is $\tau_0 \simeq 900$ s, so that neutrons with Lorentz factors $\gamma_n \gtrsim 10^8$ decay at kiloparsec distances from the center. The spectrum of neutrons at distance $r = r_{\rm kpc}$ kpc is

$$N_r(\gamma) = N_0(\gamma)\exp\left(-\frac{r}{c\tau_0\gamma_n}\right) = N_0(\gamma)\exp\left(-\frac{1.1r_{\rm kpc}}{\gamma_{n,8}}\right), \quad (5)$$

where $N_0(\gamma)$ is the spectrum of neutrons produced in the compact jet at $\lesssim$parsec scales. For a power-law injection spectrum of neutrons given by $N_0(\gamma_n) \propto \gamma_n^{-2}$, the intensity of neutron-decay electrons at distance r is equal to

$$\dot{N}_\beta(r) \simeq 2.7\times10^{46}r_{\rm kpc}^{-2}W_{n,56}\ {\rm s}^{-1}, \quad (6)$$

where $W_{n,56} = W_n/10^{56}$ ergs is the total energy in neutrons. The number of β-decay electrons $\dot{N}_\beta$ could suffice in equation (4) up to distances of $r \simeq 1$ Mpc, provided that the spectrum of neutrons in the neutral beam extends to 10^{20} eV. Note that the Lorentz factors of β-decay electrons are about the same as the Lorentz factors of the parent neutrons, i.e., $\gamma_e \gtrsim 10^8$ $r_{\rm kpc}$.

If an amount of energy W_n in UHE neutrons is ejected from the central engine during a period $\Delta t_{\rm high} \simeq 3$ kyr of high-state activity, then these neutrons form a slab of $\simeq$1 kpc length moving along the jet at nearly the speed of light. The production power of UHE neutrons $L_n \simeq W_n/\Delta t_{\rm high} \simeq 10^{45}W_{n,56}$ ergs s^{-1} could be provided if the total power of the accelerated protons in the AGN core is $\sim3\times10^{46}$ $W_{\rm n,56}$ ergs s^{-1}. This is quite acceptable for the powerful central engines of FR 2 galaxies (Rawlings & Saunders 1991).

The power requirements on the central engine are significantly more relaxed if we take into account e^+-e^- pairs produced in photoabsorption of the γ-ray component of the UHE neutral beam. These electrons are produced with Lorentz factors $\gtrsim 10^{10}$ at distances $\gg 10$ kpc (see Atoyan & Dermer 2003). Because of the relativistic KN effect, the efficiency of the electromagnetic cascade of these leptons on the CMBR is essentially suppressed in an ambient magnetic field as low as $\gtrsim 1$ μG. Indeed, the Compton cooling time of electrons with $\gamma_{10} \equiv \gamma/10^{10} \gtrsim 1$ on CMBR is $t_{\rm KN} \simeq 5\times10^4(1+z)^{-2}\gamma_{10}$ yr, while the synchrotron cooling occurs on timescales $t_{\rm syn} \simeq 1.6\times10^3(B_\perp/1\ \mu{\rm G})^{-2}\gamma_{10}^{-1}$ yr. To have an efficient cascade, Neronov et al. (2002) have assumed a jet with a magnetic field of order ≥ 10 μG (which is needed for effective synchrotron radiation), which is extremely well aligned, such that the perpendicular component of the field is very small, $B_\perp \lesssim 0.1$ μG.

In our model, in which the flux detected from X-ray knots is produced in the downstream regions of the forward shocks, we can allow significantly less ordered magnetic fields in the upstream region of the shock, with $B_\perp \sim 1$ μG. In this case the efficiency of the Compton emission, which defines the

efficiency of the cascade of pairs with initial Lorenz factors $\gamma \gtrsim 10^{10}$, would be only $t_{\rm syn}/t_{\rm KN} \lesssim 10^{-2}$. The energy of injected UHE pairs, however, is orders of magnitude larger than the energy $\gamma \gtrsim 10^8$ of e^+-e^- pairs effectively produced *in* the cascade. Furthermore, the efficiency of the Compton process rises dramatically when the synchrotron losses bring the injected electrons (of both signs) closer to $\gamma \simeq 2\times10^9$. This implies that the number of electrons produced from a single initial UHE γ-ray photon could be significantly larger than the number of β-decay electrons. Therefore, in the case of comparable powers in the neutron and γ-ray components of the neutral beam, as expected for FR 2 radio quasars (Atoyan & Dermer 2003), the total *number* of leptons with $\gamma \gg 10^7$ needed for the second electron population in the knots would be determined by the γ-ray component of the UHE neutral beam.

In the stationary-frame magnetic field $B_{\rm up\perp} \gtrsim 1$ μG upstream of the shock (corresponding to comoving $B'_{\rm up\perp} \sim \Gamma B_{\rm up\perp} \gtrsim 10$ μG), these electrons cool to energies

$$\gamma_{\rm min} \simeq 4\times10^{10}(\Delta t_{\rm kyr})^{-1}(B_{\rm up\perp}/1\ \mu{\rm G})^{-2}$$

during time $\Delta t = \Delta t_{\rm kyr}$ kyr since they were produced in the jet fluid and until they are overtaken by the trailing relativistic shock. Note that our model does not require an extremely ordered magnetic field along the jet, although stretching of the preexisting intergalactic magnetic field along the jet is a very plausible outcome of the decay of the neutral beam and appearance of the beam of charged UHE secondaries driving the extended jet. Because the time of injection for different electrons would be different, a broad spectrum of ultrarelativistic e^+-e^- pairs up to their energy at production will be overtaken. The enhanced magnetic field downstream of the shock results in rapid radiative losses, a "lighting up" of these electrons, and the appearance of an X-ray knot.

In the case of $\gamma_{2,\rm min} \gg 10^8$, a cooling synchrotron spectrum with $\alpha_{\rm X} \simeq 0.5$ is produced. A small contribution of electrons from the pair-photon cascade on the CMBR, as discussed above, could effectively result in $\gamma_{2,\rm min} \lesssim 10^8$. It may also be the result of a higher $B_{\rm up\perp}$ and a longer cooling time Δt, which in principle could reach $\gtrsim 10^5$ yr at distances greater than 100 kpc. In that case steeper synchrotron spectra at keV energies are produced, as in Figure 2.

4. DISCUSSION

The EC model for extended X-ray jets faces difficulties with large energy requirements and in explaining the different spatial profiles at radio, optical, and X-ray frequencies. It also cannot be invoked to explain knots and hot spots for which the X-ray spectral indices are significantly steeper than the radio spectral indices; in such cases a synchrotron model is favored.

The large energy requirements in the EC model can be reduced to acceptable values only by assuming Doppler factors $\delta \geq 10$. In these cases, the jet would have to be directed toward us at very small angles, only $\theta \leq 6^\circ$. Although we cannot exclude that the number of X-ray jets with such small angles could still be significant, the probability for one of the two jets of any quasar to be directed within such an angle is only $P_\theta = (1-\cos\theta)/2\pi \leq 8.7\times10^{-4}(\theta/6^\circ)^2$. Allowing for X-ray jets with $\theta \lesssim 20^\circ$ increases the probability of detecting several such sources by several orders of magnitude. A common model for X-ray knots would then have to be able to deal with sufficiently large θ to allow debeamed jets with $\delta \ll \Gamma \simeq 10$. The energy demands for such jets become unrealistic in the EC model.

The large energy requirements are significantly relaxed for synchrotron models. Synchrotron X-rays are produced by very high energy electrons with short cooling times, which minimizes the injection power of electrons needed to explain the X-ray flux. For a two-component synchrotron model, unlike for the EC model, the magnetic field is not limited by the ratio of X-ray to radio fluxes and a given inclination angle (obtained, for example, by fixing the maximum possible Doppler factor). This minimizes the total energy accumulated in the form of radio-emitting electrons and magnetic fields in the knot needed to explain the observed radio flux. The comoving equipartition fields in FR 2 knots are typically at the level $\sim$50–100 μG, which are higher than $B \sim 10$–20 μG deduced from EC models. The synchrotron interpretation of X-rays also allows one to have significantly debeamed jets and still remain within an acceptable range for the energy budget, as in the knots of 3C 273 (Fig. 1).

The relative advantage of synchrotron models for debeamed jets with $\delta \ll \Gamma$ is due essentially to the more narrow beaming diagram for the EC radiation than for the synchrotron radiation in the stationary frame (Dermer 1995). This is the case if the photons are detected at an angle $\theta \gg 1/\Gamma$. In the comoving frame such photons are produced in Compton "tail-on" collisions with beamed (in the comoving frame) external photons at angles $(1-\cos\theta') \ll 1$; therefore, the efficiency of the Compton process is strongly reduced. In the meantime, synchrotron radiation production in a quasi-isotropic knot magnetic field is isotropic in the comoving frame.

The steeper SED in the optical than X-ray bands in some knots, such as the A1 or B1 knots of 3C 273 in Figure 1, can be explained in the framework of a single population of electrons accelerated to multi-TeV energies in the shocks forming the knots (DA02). The two-component synchrotron model appears more general. In particular, it can explain practically all types of SEDs detected from the knots and hot spots of multi-kiloparsec–scale jets of FR 2 radio galaxies, such as the knot WK 7.8 of PKS 637−752, in which the optical flux is below the power-law extrapolation of fluxes from the radio to X-ray bands by more than 1 order of magnitude.

We have argued that the origins of the two different components in the knots and hot spots of FR 2 jets can be naturally explained within a unified model for large-scale jets as manifestations of neutral beams (Atoyan & Dermer 2001, 2003). These beams, composed of UHE neutrons, γ-rays, and neutrinos, are efficiently produced in the compact relativistic jets of FR 2 quasars by accelerated UHE protons in the process of photomeson interactions with the accretion disk radiation on $\lesssim$parsec scales. The decay of UHE neutrons deposits momentum and energy of the neutral beam into the intergalactic medium and drives surrounding plasma to relativistic motion (presumably with moderately relativistic speeds, although this requires a hydrodynamic study to quantify) through interactions with ambient magnetic fields and the generation of plasma waves.

The appearance of knots in continuous jets could be manifestations of shocks resulting from the increased activity of the central engine at some time in the past (Neronov et al. 2002; Atoyan & Dermer 2003). The first population of electrons is produced in the process of first-order Fermi acceleration of electrons from the surrounding intergalactic medium. The radio electrons cool slowly; therefore, they drift and accumulate along the jet, which explains the increase of radio brightness.

A second population of electrons in the jet originates in the decay of UHE γ-rays with Lorentz factors $\gamma_0 \gtrsim 10^{10}$–10^{13} eV

(Atoyan & Dermer 2003) and can be contributed even by electrons from β-decay of neutrons. It is essential that the production spectrum of these electrons be cut off at lower energies, $\gamma_C \lesssim \gamma_0$. Because of the strong KN effect for the Compton radiation of UHE electrons, most of the electron energy is deposited in the form of synchrotron radiation at MeV-GeV energies in ambient fields $B \gtrsim 1$ μG. This radiation can be effectively lost for an observer outside the jet opening angle. These electrons cool down to Lorentz factors $\gamma \gtrsim 10^8$–10^9 before being overtaken by the relativistic shock. Reprocessing even a small fraction of the γ-ray–beam energy in the pair-photon cascade along the jet, however, results in a very significant contribution to the total number of UHE electrons, with a broad spectrum above $\gamma \sim 10^8$ and a cutoff at lower energies. These electrons are deposited throughout the length of the jet and are found, in particular, in the jet fluid in front of the shock. Convection of these electrons downstream of the shock with enhanced magnetic field results in a second synchrotron component that can explain the anomalously hard X-ray SEDs of many knots. Note that this component of electrons is reenergized at the shock front in the process of adiabatic compression. Moreover, because of the high efficiency of synchrotron radiation, in many cases even the energy of the neutral beam deposited in the β-decay electrons alone could be sufficient for the explanation of the low X-ray fluxes observed. We note that MHD waves excited by the beam, as in the shear boundary-layer model of Stawarz & Ostrowski (2004), could also contribute to the reacceleration and energization of a hard electron component.

The decline of the deposition rate of UHE electrons with distance r from the AGN core could be as fast as $\propto r^{-2}$ in the case of a dominant β-decay electron contribution. The decline could be somewhat slower in the case of a significant contribution from pair-photon cascades of UHE electrons. This explains the fast decline of X-ray emission of knots along the jet. The final hot spot in our model would represent a termination shock of the relativistic flow when the jet runs out of UHE neutral-beam–decay products that sustain the forward progress of the relativistic jet into the ambient medium. Compression and additional acceleration of the second component of electrons (cooled down to $\gamma_{\rm min} \gtrsim 10^6$ on timescales up to 1 Myr for hot spots at distances $\lesssim$300 kpc) and the increase of the magnetic field in the downstream region of this relativistic jet termination shock can explain the spectrum of the hot spot of Pic A with $\alpha_X \geq 1$.

For very distant quasars with $z \gtrsim 3$, such as have been reported recently (Schwartz 2002b; Siemiginowska et al. 2003), an additional powerful channel contributing to the second electron component in large-scale jets appears. At such redshifts, the photomeson interaction length of super-GZK (Greisen-Zatsepin-Kuzmin) neutrons becomes comparable to and even less than the megaparsec scale of the jets. In this case, the input from the super-GZK neutron component of the UHE neutral beam and the efficiency of the electromagnetic cascade increases dramatically. In this way, the increased energy density of the CMBR can explain the detectability of X-rays even from quasars at large redshifts (compare the different ideas of Schwartz [2002a] for the EC model).

We propose two testable predictions of this scenario. The first is variability of the X-ray flux from the knots of FR 2 radio galaxies. This possibility, suggested by observations of X-ray variability in the knots of M87 (Perlman et al. 2003), is a consequence of the short cooling timescale $t_{\rm syn} \simeq 500[(1+z)/E_{\rm keV}\delta B_{30}^3]^{1/2}$ yr of X-ray–emitting electrons. For the comoving magnetic fields in the knots (and hot spots) reaching $B' \gtrsim 100$ μG, this time can be $\lesssim 50/(E_{\rm keV})^{1/2}$ yr even for knots or jets with moderate Doppler factors, $\delta \lesssim 3$, moving at rather large angles, $\theta \lesssim 20^\circ$. One could then expect that variations of the injection rate of electrons at the shock (swept up in the upstream region) on timescales $t_{\rm var} \gtrsim t_{\rm syn}$ would result in variations of the X-ray flux on the same scales. Detection of variability could be feasible for X-ray knots with transverse sizes $\lesssim$1 kpc, which are sufficiently thin (flat) along our line of sight. The detection of a small-amplitude variability (at the level of up to several percent over reasonable observation times) depends on the strength of the magnetic field downstream of the shock. For knots detected with *Chandra* at X-ray count rates $\gtrsim 100$ hr^{-1}, like those from knot WK 7.8 in PKS 0637−752 (Chartas et al. 2000), simple estimates show that statistically significant flux variations could be expected for observations separated by several years. X-ray variability of an FR 2 knot or hot spot would be difficult to understand in the context of the EC model with the long cooling times of the emitting electrons and stationary target for Compton interactions.

A second prediction is that high-energy ($\gtrsim 10^{14}$ eV) neutrinos will be detected from core-dominated quasars with kilometer-scale neutrino telescopes such as IceCube. Detection of every such neutrino from a flat-spectrum radio quasar such as 3C 279 implies that a total energy $\sim 5 \times 10^{54} \delta^{-2} d_{28}^2$ ergs is injected in the inner jet on sub-kiloparsec scales (Atoyan & Dermer 2003). Therefore, even the detection of one neutrino per year would imply a UHE neutral-beam power of $\sim 10^{46} \delta^{-2} d_{28}^2$ ergs s^{-1}.

Finally, we note that this model is developed in view of a scenario (Böttcher & Dermer 2002; Cavaliere & D'Elia 2002) in which radio-loud AGNs are formed by merging IR-luminous galaxies and evolve from a high-luminosity FR 2–quasar phase at early cosmic times to a lower luminosity FR 1–BL Lac phase at later times, thus explaining the sequence of flat-spectrum radio quasar and BL Lac object SEDs (Fossati et al. 1998). The crucial features in this scenario are the amount of broad-line–emitting gas that fuels the AGN and the corresponding intensities of the external radiation field in the vicinity of the inner jet. This radiation field determines the power of the neutral beam that produces the distinctive lobe-dominated morphologies of FR 2 radio galaxies and, in exceptional cases such as Pic A, a linear jet (Wilson et al. 2001). FR 1 galaxies, where the neutral-beam power is negligible, consequently display very different radio jet morphologies.

We thank Herman Marshall, Eric Perlman, and Andrew Wilson for comments and discussions and the referee for useful comments. A. A. appreciates the hospitality of the NRL High Energy Space Environment Branch during his visit, when this work was started. The work of C. D. D. is supported by the Office of Naval Research and *GLAST* Science Investigation DPR-S-1563-Y.

REFERENCES

Aharonian, F. 2002, MNRAS, 332, 215
Atoyan, A. M., & Dermer, C. D. 2001, Phys. Rev. Lett., 87, 221102
———. 2003, ApJ, 586, 79
Böttcher, M., & Dermer, C. D. 2002, ApJ, 564, 86
Cavaliere, A., & D'Elia, V. 2002, ApJ, 571, 226
Celotti, A., & Fabian, A. C. 1993, MNRAS, 264, 228

Celotti, A., Ghisellini, G., & Chiaberge, M. 2001, MNRAS, 321, L1
Chartas, G., et al. 2000, ApJ, 542, 655
Conway, R. G., & Davis, R. J. 1994, A&A, 284, 724
Dermer, C. D. 1995, ApJ, 446, L63
Dermer, C. D., & Atoyan, A. M. 2002, ApJ, 568, L81 (DA02)
———. 2004, ApJ, 611, L9
Dermer, C. D., & Schlickeiser, R. 2002, ApJ, 575, 667
Dermer, C. D., Sturner, S. J., & Schlickeiser, R. 1997, ApJS, 109, 103
Fossati, G., Maraschi, L., Celotti, A., Comastri, A., & Ghisellini, G. 1998, MNRAS, 299, 433
Georganopoulos, M., & Kazanas, D. 2004, ApJ, 604, L81
Ghisellini, G., & Celotti, A. 2001, MNRAS, 327, 739
Hardcastle, M. J., Birkinshaw, M., & Worrall, D. M. 2001, MNRAS, 326, 1499
Harris, D. E., & Krawczynski, H. 2002, ApJ, 565, 244
Marshall, H. L., Miller, B. P., Davis, D. S., Perlman, E. S., Wise, M., Canizares, C. R., & Harris, D. E. 2002, ApJ, 564, 683
Marshall, H. L., et al. 2001, ApJ, 549, L167
Mukherjee, R., & Chiang, J. 1999, Astropart. Phys., 11, 213
Neronov, A., Semikoz, D., Aharonian, F., & Kalashev, O. 2002, Phys. Rev. Lett. 89, 051101
Perlman, E. S., Harris, D. E., Biretta, J. A., Sparks, W. B., & Macchetto, F. D. 2003, ApJ, 599, L65
Rawlings, S., & Saunders, R. 1991, Nature, 349, 138
Roland, J., Teyssier, R., & Roos, N. 1994, A&A, 290, 357
Sambruna, R. M., Urry, C. M., Tavecchio, F., Maraschi, L., Scarpa, R., Chartas, G., & Muxlow, T. 2001, ApJ, 549, L161
Schwartz, D. A. 2002a, ApJ, 569, L23
———. 2002b, ApJ, 571, L71
Schwartz, D. A., et al. 2000, ApJ, 540, L69
Siemiginowska, A., Bechtold, J., Aldcroft, T. L., Elvis, M., Harris, D. E., & Dobrzycki, A. 2002, ApJ, 570, 543
Siemiginowska, A., Smith, R. K., Aldcroft, T. L., Schwartz, D. A., Paerels, F., & Petric, A. O. 2003, ApJ, 598, L15
Stawarz, Ł. 2004, Chin. J. Astron. Astrophys., in press (astro-ph/0310795)
Stawarz, Ł., & Ostrowski, M. 2002, ApJ, 578, 763
Stawarz, Ł., Sikora, M., Ostrowski, M., & Begelman, M. C. 2004, ApJ, 608, 95
Tavecchio, F., Ghisellini, G., & Celotti, A. 2003, A&A, 403, 83
Tavecchio, F., Maraschi, L., Sambruna, R. M., & Urry, C. M. 2000, ApJ, 544, L23
Wilson, A. S., & Yang, Y. 2002, ApJ, 568, 133
Wilson, A. S., Young, A. J., & Shopbell, P. L. 2000, ApJ, 544, L27
———. 2001, ApJ, 547, 740